LETTERS
https://doi.org/10.1038/s41565-018-0267-z
nature nanotechnology

Bacteria photosensitized by intracellular gold nanoclusters for solar fuel production

Hao Zhang[1,7], Hao Liu[1,7], Zhiquan Tian[1,2], Dylan Lu[1,3], Yi Yu[1,4], Stefano Cestellos-Blanco[5], Kelsey K. Sakimoto[1] and Peidong Yang[1,3,5,6*]

The demand for renewable and sustainable fuel has prompted the rapid development of advanced nanotechnologies to effectively harness solar power. The construction of photosynthetic biohybrid systems (PBSs) aims to link preassembled biosynthetic pathways with inorganic light absorbers. This strategy inherits both the high light-harvesting efficiency of solid-state semiconductors and the superior catalytic performance of whole-cell microorganisms. Here, we introduce an intracellular, biocompatible light absorber, in the form of gold nanoclusters (AuNCs), to circumvent the sluggish kinetics of electron transfer for existing PBSs. Translocation of these AuNCs into non-photosynthetic bacteria enables photosynthesis of acetic acid from CO_2. The AuNCs also serve as inhibitors of reactive oxygen species (ROS) to maintain high bacterium viability. With the dual advantages of light absorption and biocompatibility, this new generation of PBS can efficiently harvest sunlight and transfer photogenerated electrons to cellular metabolism, realizing CO_2 fixation continuously over several days.

Although the conversion efficiencies of inorganic semiconductor devices from solar to different energy forms can easily surpass 20%, the transduction of solar energy into specific organics remains a bottleneck for abiotic catalysts[1,2]. The construction of PBSs enables solar-to-chemical energy conversion with high specificity and low cost[3]. Among several well-documented prototypes of hybrid inorganic–biological systems for photosynthetic CO_2 fixation[4–6], the whole-cell strategy is favoured because of the involvement of a complete biological CO_2 reduction cycle and the ability to self-replicate and self-repair[7] (Fig. 1). Non-photosynthetic organisms, especially those developed in modern synthetic biology, possess more desirable metabolic pathways than their photosynthetic counterparts, offering a tunable CO_2 metabolism for diverse products[8]. Our proof-of-concept whole-cell hybrid system was realized by interfacing the non-photosynthetic electrotrophic bacterium *Sporomusa ovata* with a photoelectrochemical silicon nanowire array[4]. *Sporomusa ovata* can directly use electrons from the silicon photoelectrode through the bio-inorganic interface assisted by numerous active enzymes and functional proteins on their membranes[9]. Recently, we demonstrated that the acetogenic bacterium *Moorella thermoacetica* (ATCC 39073) can self-precipitate cadmium sulfide (CdS) nanoparticles on its membrane[7]. The photo-excited electrons from CdS nanoparticles are captured by membrane proteins to produce reducing equivalents that are ultimately transported into the cytoplasm to drive the Wood–Ljungdahl pathway for CO_2 fixation. In both examples, intimate bio–inorganic interfaces are formed between the inorganic semiconductors and the bacteria. Nevertheless, as most biocatalytic CO_2 fixation cycles are carried out in the cytoplasm, mass transport of redox shuttle molecules across the membrane into the cytoplasm would consume extra energy and be bottlenecked by transmembrane diffusion[10]. Therefore, simultaneous generation of photo-excited electrons and reducing equivalents inside the bacteria should improve the efficiency of energy transduction. An essential prerequisite for the light absorber is the ability to be taken up by living microorganisms without losing its chemical integrity.

Here we introduce ultra-small AuNCs as the biocompatible intracellular photosensitizer for non-photosynthetic bacteria. AuNCs possess chromophore-like discrete energy states and unique geometric structures[11]. The tunability of the core size and surface ligands of the AuNCs allows us to manipulate their biochemical/biophysical properties such as cell uptake, cytotoxicity, biocompatibility and molecular electronic structures[12–14]. In particular, strides have been made in the use of AuNCs in solar light harvesting as a visible-light absorber in the form of a type II junction[15]. Proof-of-concept studies have demonstrated that AuNCs can be delivered into mammalian cells either in vivo or in vitro to achieve cell imaging with high biocompatibility[16,17].

Incorporation of Au nanoclusters into *M. thermoacetica*

Water-soluble AuNCs (majority $Au_{22}(SG)_{18}$, where SG is glutathione) were synthesized following a procedure reported previously, with slight modification ($Au_{22}(SG)_{18}$ content ~92%)[18,19]. *Moorella thermoacetica* bacteria were inoculated and cultured in heterotrophic medium for 2 days before the $Au_{22}(SG)_{18}$ solution was injected (see Methods for details). In the following 2 days, the bacteria underwent exponential growth in the presence of AuNCs. They were then centrifuged, separated from the supernatant and redispersed in autotrophic medium. In Supplementary Fig. 2, the redispersed solution shows almost the same colour as before the centrifugation, whereas the supernatant is clear, suggesting that AuNCs were preferentially taken up by *M. thermoacetica* with a 95.37% uptake efficiency (see Supplementary Information). Furthermore, the ultraviolet–visible (UV–vis) absorption spectrum of the redispersed *M. thermoacetica*/AuNC solution displays the same characteristic peaks as the bare AuNC solution, in contrast to the featureless absorption curve of the bare *M. thermoacetica* solution (Supplementary Fig. 3), indicating that the AuNCs remain intact during the integration process.

[1]Department of Chemistry, University of California, Berkeley, Berkeley, CA, USA. [2]Key Laboratory of Analytical Chemistry for Biology and Medicine (Ministry of Education), College of Chemistry and Molecular Sciences, Wuhan University, Wuhan, P. R. China. [3]Chemistry Sciences Division, Lawrence Berkeley National Laboratory, Berkeley, CA, USA. [4]School of Physical Science and Technology, ShanghaiTech University, Shanghai, China. [5]Department of Materials Science and Engineering, University of California, Berkeley, Berkeley, CA, USA. [6]Kavli Energy NanoSciences Institute, Berkeley, CA, USA. [7]These authors contributed equally: Hao Zhang, Hao Liu. *e-mail: p_yang@berkeley.edu

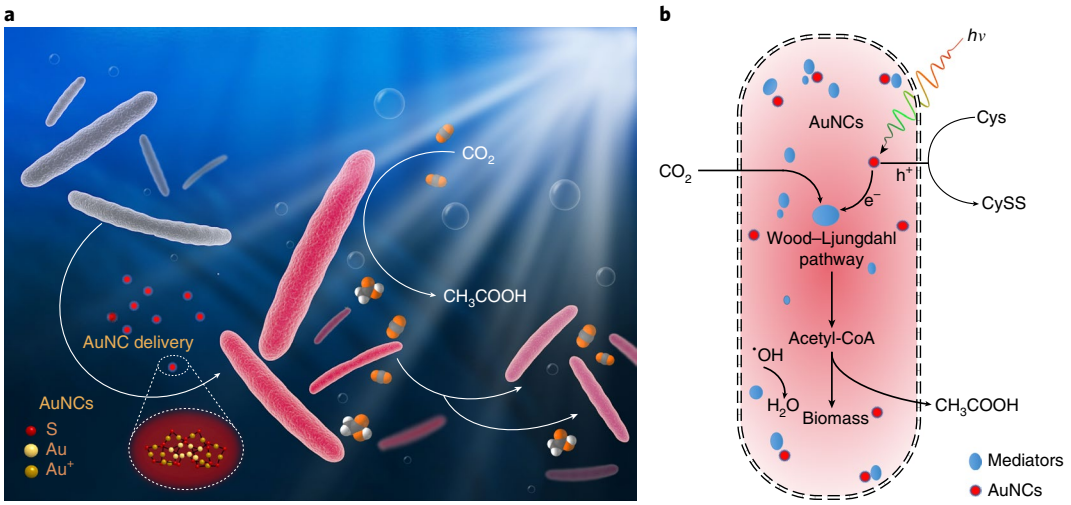

Fig. 1 | Schematic diagram of the *M. thermoacetica*/AuNC hybrid system. a, The $Au_{22}(SG)_{18}$ nanoclusters were delivered into bare *M. thermoacetica* (grey) during the culture process, forming *M. thermoacetica*/AuNCs with red emission. The simulated chemical structure of $Au_{22}(SG)_{18}$ nanoclusters is shown in the inset[18]. Light yellow spheres, Au atoms in the core; dark yellow, Au atoms in the staple motifs; red, S atoms in the shell. All other atoms (carbon, hydrogen) have been omitted from this structure for clarity. Also shown are space-filling models of acetic acid and CO_2 (orange, oxygen; grey, carbon; white, hydrogen). **b**, Schematic of bacterium. The electrons generated from intracellular AuNCs under illumination are used by enzymatic mediators inside the cytoplasm and are finally passed on to the Wood–Ljungdahl pathway. Hypothesized electron transfer pathways are presented in Supplementary Fig. 1.

Structure illumination microscopy (SIM) was further used to clarify the location of AuNCs in the hybrid biosystem by collecting the emissive fluorescence from AuNCs under excitation at 540 nm (Fig. 2a)[20]. Figure 2b displays the image of several AuNC-treated *M. thermoacetica* on different focal planes with a step increment of 86 nm along the *z* direction. This shows the emission intensity profile from the bottom through the top cross-sections of the bacteria. A movie of the reconstructed 3D model of an individual AuNC-treated *M. thermoacetica* is available in the Supplementary Information. To draw a solid conclusion, the same culturing conditions were also applied to the bare *M. thermoacetica* and to *M. thermoacetica* with membrane-bound CdS (*M. thermoacetica*–CdS) PBS. As a control, the bare *M. thermoacetica* display no photoluminescence emission and result in a completely dark image under 540-nm illumination (Supplementary Fig. 4). In comparison (Fig. 2c,d), SIM images of the *M. thermoacetica*–CdS PBS excited at 408 nm show greenish photoluminescence emission with an annular shape from the membrane-bound CdS nanoparticles. The distinct SIM photoluminescence emission patterns confirm the successful transportation of AuNCs into the cytoplasm of *M. thermoacetica*. Additionally, high-angle annular dark-field scanning transmission electron microscopy (HAADF-STEM) and energy-dispersive X-ray spectroscopy (EDS) mapping were performed to verify the location of the AuNCs (Fig. 2e,f,g). As shown in Fig. 2f, gold was mostly detected and well distributed across the whole bacterium without obvious aggregation on the membrane. Although the mechanism of AuNC delivery into the bacteria remains to be fully explored, the well-documented specific uptake of various metal nanoparticles and quantum dots into mammalian cells can provide clues. To be taken up specifically by living cells, nano-sized particles become chemically linked to biorecognition molecules such as peptides, antibodies, nucleic acids or small-molecule ligands[21,22]. We hypothesize that the specific AuNC uptake by *M. thermoacetica* is similarly mediated by the AuNC tripeptide surface ligand, glutathione, which has strong bioaffinity, through passive targeting[23,24].

Photosynthesis of *M. thermoacetica*/AuNC hybrid system

After successful incorporation of AuNCs into living bacteria, we examined the photosynthetic ability of the hybrid system. Before being exposed to low-intensity simulated sunlight (calibrated by photodiode, air mass 1.5 global spectrum (AM 1.5), 2 W m^{-2}), the heterotrophic medium was replaced by autotrophic medium, to make sure that CO_2 was the only external carbon source for *M. thermoacetica*. As the only respiration product, the concentration of acetic acid was monitored by quantitative proton nuclear magnetic resonance (^{1}H-qNMR) (Supplementary Fig. 5), and ^{13}C isotope labelling was also carried out to track the carbon source during the photosynthesis (Supplementary Fig. 6). Several controls in terms of the number of cells and culture volume with the optimized light absorber concentration for *M. thermoacetica*/AuNCs and *M. thermoacetica*–CdS PBSs were carried out. The results show that these two hybrids are capable of fixing CO_2 to generate acetic acid under illumination. The acetic acid yield was normalized to the dry weight after photosynthesis for each system (Supplementary Information), thus taking cell population, cell phases and toxicity effects of photosensitizers into account. In the two deletional controls, namely bare *M. thermoacetica* in the light and *M. thermoacetica*/AuNCs in the dark, the acetic acid yield is negligible (Fig. 3a). The *M. thermoacetica*/AuNC system exhibits faster acetic acid production than the *M. thermacetica*–CdS system. After 4 days, the accumulated acetic acid yield of *M. thermoacetica*/AuNCs is noticeably higher than that of the *M. thermoacetica*–CdS system. To illustrate the photosensitizing behaviour of AuNCs inside *M. thermoacetica*, we used photoluminescence spectroscopy to study the electron transfer between the AuNCs and the bacteria (Fig. 3b). The bare AuNC solution shows strong red and near-infrared photoluminescence emission centred at 680 nm when excited by a 532-nm solid-state laser beam, while the bare *M. thermoacetica* solution shows no photoluminescence emission. Before carrying out the photosynthesis, the photoluminescence emission spectrum of the *M. thermoacetica*/AuNCs in the CO_2-free medium gives a broad peak with slight redshift and lower intensity than the bare AuNC solution. However, during the photosynthetic process, the red photoluminescence emission of the *M. thermoacetica*/AuNCs solution is totally quenched. Thus, we argue that instead of undergoing a recombination process, photoexcited electrons from the AuNCs are transferred to cytoplasm-distributed redox mediators, such as ferredoxin (Fd), flavoproteins (Fp) and rubredoxins (Rd) (Supplementary Table 1) as illustrated in

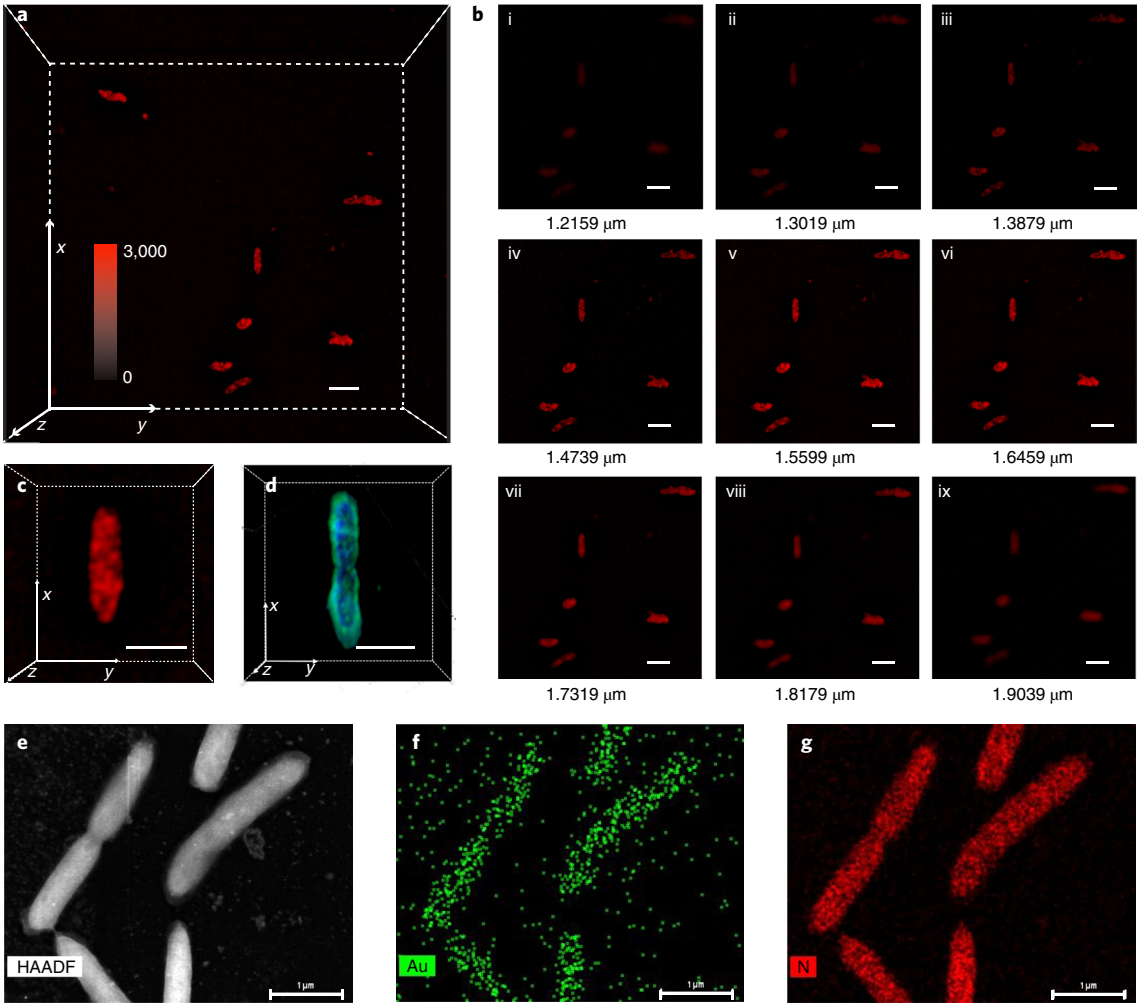

Fig. 2 | Microscopy images of the M. thermoacetica/AuNC hybrid system. **a**, SIM image of several *M. thermoacetica*/AuNCs fluorescing in red (excitation at 540 nm) with total counts ranging from 0 to 3,000. **b**, SIM images of different focal planes (numbered successively i to ix) along the *z* direction. **c**, SIM image of individual *M. thermoacetica*/AuNC PBS. **d**, SIM image of a single *M. thermoacetica*–CdS PBS (excitation at 408 nm) with annular-shaped emission. **e**, HAADF-STEM image of *M. thermoacetica*/AuNCs. **f**, **g**, EDS mapping of the region in **e**, showing the elements (**f**) Au and (**g**) N across the entire cell. Scale bars for **a**–**d**, 2 μm.

previous enzymological and thermodynamic studies on the same bacterium[25,26]. Moreover, an average lifetime of 729 ns was determined for the luminescence decay at 630 nm for the bare AuNC solution (Supplementary Fig. 7), which results from ligand-to-metal charge transfer relaxation occurring at a triplet metal-centred state in the long, interlocked gold shell[27]. The ultra-long photoluminescence lifetime is beneficial for electron transfer from the AuNCs to the energy transfer system (ETS) in the cytoplasm[28]. Ultimately, the photo-excited electrons from AuNCs are passed on to the Wood–Ljungdahl pathway to synthesize acetic acid from CO_2, while the holes are quenched by cysteine, resulting in its oxidized form, cystine (CySS)[7]. The overall photosynthetic reaction is

$$2CO_2 + 8Cys + 8h\nu \xrightarrow{M.\ thermoacetica/AuNCs} CH_3COOH + 2H_2O + 4CySS \quad (1)$$

To further study the photosynthetic behaviour, we illuminated *M. thermoacetica*/AuNC hybrids in an alternating light–dark cycle of 12 hours each, to imitate the intermittent nature of the solar source. In Fig. 3c, we can see continuous production of acetic acid during the day–night cycles, mainly due to the accumulation of metabolic intermediates as illustrated in our previous study[7], which could be confirmed by the observation of distinct increases in the rate of acetic acid production for dark cycles. The lower acetic acid increase in the first dark cycle, compared with that of the following dark cycles, indicates a potential deficit of the accumulated biosynthetic intermediates at the beginning, and the possible explanation lies in insufficient energy generated or rapid consumption of biomass. The quantum efficiency was quantified daily by the ratio of the effective electrons used for acetic acid production to the total input photon flux (Supplementary Information). The overall quantum efficiency can be as high as (2.86 ± 0.38)% for the first day, 33% higher than *M. thermoacetica*–CdS with (2.14 ± 0.16)%, reflecting better CO_2 fixation ability in *M. thermoacetica*/AuNCs system. Additionally, although natural photosynthesis can produce organic compounds by CO_2 fixation during the daytime, most of these are consumed by the respiration process at night. The photosynthetic product of *M. thermoacetica*/AuNCs PBS, acetic acid, cannot be catabolized by *M. thermoacetica*, and thus the catabolic energy loss in the dark cycles is absent. This special behaviour could potentially help the PBS to outstrip the efficiency of natural photosynthesis.

Both the continuous and the light–dark cycle experiment reveal that the rate of acetic acid production began to plateau after

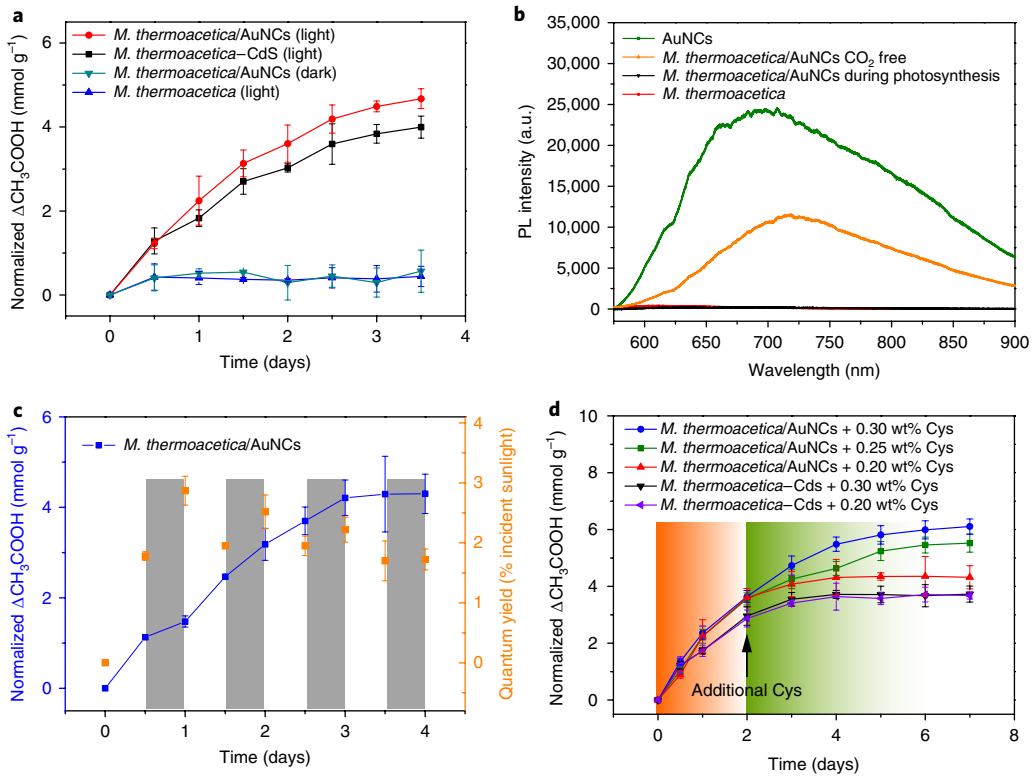

Fig. 3 | Photosynthesis behaviour of different systems. a, Normalized photosynthetic production of acetic acid by *M. thermoacetica*, *M. thermoacetica*/AuNCs and *M. thermoacetica*–CdS PBSs under continuous low-intensity illumination and in dark conditions ($n = 20$ culture batches for *M. thermoacetica*–CdS (light), $n = 35$ culture batches for other conditions). **b**, Photoluminescence (PL) spectra of pure AuNCs, bare *M. thermoacetica*, *M. thermoacetica*/AuNCs in CO_2-free conditions without photosynthesis ability, and *M. thermoacetica*/AuNCs in the photosynthesis process. **c**, Normalized acetic acid production and quantum yield of *M. thermoacetica*/AuNCs as percentage of incident light, during light–dark cycles ($n = 21$ culture batches). **d**, Cysteine-dependent acetic acid yield in *M. thermoacetica*/AuNCs and *M. thermoacetica*–CdS with cysteine added at day 2, for 7 days of photosynthesis ($n = 12$ culture batches). All points and error bars show the mean and standard deviation, respectively, of the experiments.

3 days. We postulated that the sacrificial hole scavenger, Cys, was quickly consumed by the *M. thermoacetica*/AuNCs PBS during the first 3 days of photosynthesis. Therefore, a second injection of Cys in varying amounts was made on day 2. In Fig. 3d, the accumulated acetic acid production normalized by dry weight after a week of photosynthesis reached 4.51 mmol g^{-1}, 5.52 mmol g^{-1} and 6.01 mmol g^{-1} when the overall feed of Cys was 0.2 wt%, 0.25 wt% and 0.3 wt%, respectively. In contrast, the addition of extra Cys in the *M. thermoacetica*–CdS PBS did not improve the acetic acid production. This can be explained by the structural instability of membrane-bound CdS nanoparticles, as shown by the observation of severe ripening and ultimately peeling off from the membranes, and the successive photo-oxidization of CdS under long illumination. The acetic acid upsurge (around 80%) in the *M. thermoacetica*/AuNC system affirms its ability to conduct a continuous solar-to-chemical conversion process.

Viability of *M. thermoacetica* in hybrid systems

The viability of bacteria in different systems was also determined by bacteria enumeration with a Petroff–Hauser counting chamber in both dark and light conditions (Fig. 4a,b). First, in the dark incubator, bacteria were cultured in parallel in heterotrophic media for 2 days, and AuNC solution, Cd^{2+} precursor solution and blank water with the same volume were then added accordingly. After continuing to increase for 12 hours, the bare *M. thermoacetica* and *M. thermoacetica*/AuNC systems maintained a relative high proliferation rate and cell viability until the fourth day, whereas the cell population of the *M. thermoacetica*–CdS system started to decline (Fig. 4a). This observation confirms the superior biocompatibility of the AuNCs. On the other hand, under the conditions of photosynthesis, we found that the bacteria population continued to increase in the first 12 hours, probably resulting from the completed division of already doubled but not yet split bacteria. Thereafter, the population of viable bare *M. thermoacetica* dropped quickly, owing to the lack of heterotrophic substrates and potential photo-oxidative degradation. The viability of *M. thermoacetica*-CdS PBS declined after day 1 and cell concentration decreased to ~25% after 4 days (from the initial $(8.9 \pm 0.2) \times 10^7$ cell ml^{-1}). Nevertheless, the cell ratio of *M. thermoacetica*/AuNCs remained higher than 100% for the first 2 days, after which the cell amount slowly dropped to ~70% (from the initial $(11.5 \pm 0.2) \times 10^7$ cell ml^{-1}).

Besides low toxicity and good biocompatibility, AuNCs are also reported to possess the ability to quench ROS[24], such as NO• and •OH, generated from the photo-oxidative degradation of metal-cluster-containing biomolecules under illumination[29]. The viability of *M. thermoacetica* could drop significantly as intracellular ROS accumulate. Therefore, we applied a ROS assay kit (MAK143) to assay the ROS level in the cytoplasm of *M. thermoacetica* by recording the intensity of ROS-triggered fluorescence emission. As shown in Fig. 4c, the ROS concentration in bare *M. thermoacetica* is 1.8 times higher than it is in *M. thermoacetica*/AuNCs after they were illuminated for 48 hours. These differences reveal the beneficial effect of AuNCs on eliminating ROS in the *M. thermoacetica*/AuNC system[30,31]. ROS scavenging by AuNCs might be attributable to its chemical catalytic property, which triggers reactions between cysteine and radicals. The AuNCs, with their multiple energy levels, are

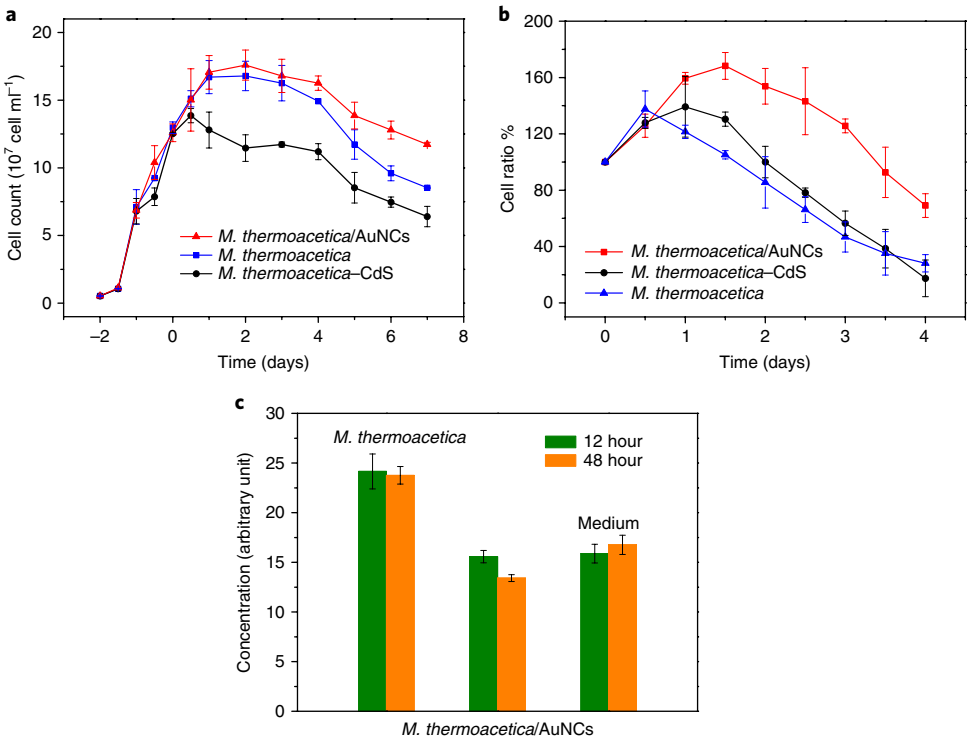

Fig. 4 | Viability measurements. a, **b**, Bacteria enumeration of *M. thermoacetica*/AuNCs, *M. thermoacetica*–CdS and bare *M. thermoacetica* by colony counting in the heterotrophic medium (**a**) in dark conditions and (**b**) in the autotrophic medium exposed to low-intensity illumination ($n = 20$ culture batches for each condition). **c**, ROS concentration of bare *M. thermoacetica*, *M. thermoacetica*/AuNCs and medium, under low-intensity illumination for 12 h and 48 h ($n = 9$). All points and error bars show the mean and standard deviation, respectively, of the experiments.

speculated to aid electron transfer to neutralize the active species to stable states[32].

Conclusions

In summary, we have shown that AuNCs, acting as an intercellular photosensitizer, could enable the non-photosynthetic bacterium, *M. thermoacetica*, to achieve efficient photosynthesis. Small AuNCs with high biocompatibility inside the bacterium enable the photosynthesis of acetic acid from CO_2. Moreover, the photogenerated electrons from intracellular AuNCs could be passed to cytoplasmic mediators by the Wood–Ljungdhal pathway, bypassing the slow mass transport and energy consumption across the cell membrane. Besides the intracellular energy transfer, continuous CO_2 fixation over 6 days benefited from the high viability of *M. thermoacetica*/AuNCs, with AuNCs acting as a ROS scavenger.

Online content

Any methods, additional references, Nature Research reporting summaries, source data, statements of data availability and associated accession codes are available at https://doi.org/10.1038/s41565-018-0267-z.

Received: 7 March 2018; Accepted: 23 August 2018;
Published online: 1 October 2018

References

1. Blankenship, R. E. et al. Comparing photosynthetic and photovoltaic efficiencies and recognizing the potential for improvement. *Science* **332**, 805–809 (2011).
2. Appel, A. M. et al. Frontiers, opportunities, and challenges in biochemical and chemical catalysis of CO_2 fixation. *Chem. Rev.* **113**, 6621–6658 (2013).
3. Sakimoto, K. K., Kornienko, N. & Yang, P. Cyborgian material design for solar fuel production: the emerging photosynthetic biohybrid systems. *Acc. Chem. Res.* **50**, 476–481 (2017).
4. Liu, C. et al. Nanowire-bacteria hybrids for unassisted solar carbon dioxide fixation to value-added chemicals. *Nano. Lett.* **15**, 3634–3639 (2015).
5. Malvankar, N. S. & Lovley, D. R. Microbial nanowires for bioenergy applications. *Curr. Opin. Biotechnol.* **27**, 88–95 (2014).
6. Liu, C., Colon, B. C., Ziesack, M., Silver, P. A. & Nocera, D. G. Water splitting—biosynthetic system with CO_2 reduction efficiencies exceeding photosynthesis. *Science* **352**, 1210–1213 (2016).
7. Sakimoto, K. K., Wong, A. B. & Yang, P. Self-photosensitization of nonphotosynthetic bacteria for solar-to-chemical production. *Science* **351**, 74–77 (2016).
8. Gronenberg, L. S., Marcheschi, R. J. & Liao, J. C. Next generation biofuel engineering in prokaryotes. *Curr. Opin. Chem. Biol.* **17**, 462–471 (2013).
9. Lovley, D. R. Powering microbes with electricity: direct electron transfer from electrodes to microbes. *Environ. Microbiol. Rep.* **3**, 27–35 (2011).
10. Silhavy, T., Kahne, D. & Walker, S. The bacterial cell envelope. *Cold Spring Harb. Perspect. Biol.* **2**, 1–16 (2010).
11. Chen, L. Y., Wang, C. W., Yuan, Z. & Chang, H. T. Fluorescent gold nanoclusters: recent advances in sensing and imaging. *Anal. Chem.* **87**, 216–229 (2015).
12. Mathew, A. & Pradeep, T. Noble metal clusters: applications in energy, environment, and biology. *Part. Part. Syst. Charact.* **31**, 1–37 (2014).
13. Zhang, X. D. et al. Ultrasmall glutathione-protected gold nanoclusters as next generation radiotherapy sensitizers with high tumor uptake and high renal clearance. *Sci. Rep.* **5**, 8669 (2015).
14. Abbas, M. A., Kamat, P. V. & Bang, J. H. Thiolated gold nanoclusters for light energy conversion. *ACS Energy Lett.* **3**, 840–854 (2018).
15. Abbas, M. A., Kim, T. Y., Lee, S. U., Kang, Y. S. & Bang, J. H. Exploring interfacial events in gold-nanocluster-sensitized solar cells: insights into the effects of the cluster size and electrolyte on solar cell performance. *J. Am. Chem. Soc.* **138**, 390–401 (2016).
16. Wang, J. et al. In vivo self-bio-imaging of tumors through in situ biosynthesized fluorescent gold nanoclusters. *Sci. Rep.* **3**, 1–6 (2013).
17. Durgadas, C. V., Sharma, C. P. & Sreenivasan, K. Fluorescent gold clusters as nanosensors for copper ions in live cells. *Analyst* **136**, 933–940 (2011).
18. Xie, J. et al. Identification of a highly luminescent $Au_{22}(SG)_{18}$ nanocluster. *J. Am. Chem. Soc.* **136**, 1246–1249 (2014).
19. Zhang, C. et al. Mimicking pathogenic invasion with the complexes of $Au_{22}(SG)_{18}$-engineered assemblies and folic acid. *ACS Nano* **12**, 4408–4418 (2018).
20. Huang, B., Babcock, H. & Zhuang, X. Breaking the diffraction barrier: super-resolution imaging of cells. *Cell* **143**, 1047–1058 (2010).

21. Medintz, I. L., Uyeda, H. T., Goldman, E. R. & Mattoussi, H. Quantum dot bioconjugates for imaging, labelling and sensing. *Nat. Mater.* **4**, 435–446 (2005).
22. Chithrani, B. D. & Chan, W. C. W. Elucidating the mechanism of cellular uptake and removal of protein-coated gold nanoparticles of different sizes and shapes. *Nano. Lett.* **7**, 1542–1550 (2007).
23. Kong, L. et al. Biocompatible glutathione-capped gold nanoclusters for dual fluorescent sensing and imaging of copper(II) and temperature in human cells and bacterial cells. *Microchim. Acta.* **183**, 2185–2195 (2016).
24. Lin, J., Zhang, H., Chen, Z. & Zheng, Y. Penetration of lipid membranes by gold nanoparticles: insights into cellular uptake, cytotoxicity, and their relationship. *ACS Nano* **4**, 5421–5429 (2010).
25. Kornienko, N. et al. Spectroscopic elucidation of energy transfer in hybrid inorganic–biological organisms for solar-to-chemical production. *Proc. Natl Acad. Sci. USA* **113**, 11750–11755 (2016).
26. Deutzmann, J. S., Sahin, M. & Spormann, A. M. Extracellular enzymes facilitate electron uptake in biocorrosion and bioelectrosynthesis. *mBio* **6**, 1–8 (2015).
27. Pyo, K. et al. Ultrabright luminescence from gold nanoclusters: rigidifying the Au(I)-thiolate shell. *J. Am. Chem. Soc.* **137**, 8244–8250 (2015).
28. Das, A. & Ljungdahl, L. G. in *Biochemistry and Physiology of Anaerobic Bacteria* (eds. Ljungdahl, L. G. et al.) 191–204 (Springer, New York, 2003).
29. Jiang, Y. et al. Light-induced N_2O production from a non-heme iron-nitrosyl dimer. *J. Am. Chem. Soc.* **136**, 12524–12527 (2014).
30. Santiago-Gonzalez, B. et al. Permanent excimer superstructures by supramolecular networking of metal quantum clusters. *Science* **353**, 571–575 (2016).
31. Xiong, B., Xu, R., Zhou, R., He, Y. & Yeung, E. S. Preventing UV induced cell damage by scavenging reactive oxygen species with enzyme-mimic Au–Pt nanocomposites. *Talanta* **120**, 262–267 (2014).
32. Gao, Y., Shao, N., Pei, Y., Chen, Z. & Zeng, X. C. Catalytic activities of subnanometer gold clusters (Au_{16}–Au_{18}, Au_{20}, and Au_{27}–Au_{35}) for CO oxidation. *ACS Nano* **5**, 7818–7829 (2011).

Acknowledgements

This work was supported by Director, Office of Science, Office of Basic Energy Sciences, Chemical Sciences, Geosciences, and Biosciences Division, of the US Department of Energy under contract no. DE-AC02-05CH11231, FWP no. CH030201 (Catalysis Research Program). We thank the imaging facilities at the National Center for Electron Microscopy (NCEM) at the Molecular Foundry and the NMR facility of the College of Chemistry, University of California, Berkeley. Work at the NCEM was supported by the Office of Science, Office of Basic Energy Sciences, of the US Department of Energy under contract no. DE-AC02-05CH11231. Research reported in this publication was supported in part by the National Institutes of Health S10 programme under award no. 1S10OD018136-01. The content is solely the responsibility of the authors and does not necessarily represent the official views of the National Institutes of Health. H.Z. thanks the Suzhou Industry Park (SIP) fellowship.

Author contributions

H.Z., H.L. and P.Y. designed the studies and prepared the manuscript. H.L. synthesized the AuNCs. H.Z. and Z.T. cultured the bacteria and carried out all the photosynthesis experiments. H.L. and S.C.-B. repeated the photosynthesis experiments and confirmed the reproducibility. H.Z. performed the UV–vis absorption, SIM imaging and bacteria enumeration characterization. D.L. and H.Z. conducted photoluminescence emission spectrum measurements. Y.Y. conducted the HAADF-STEM characterization. S.C.-B. helped with the fluorescence reader for the ROS test. K.K.S. provided discussion. All authors discussed the results and commented on the manuscript.

Competing interests

The authors declare no competing interests.

Additional information

Supplementary information is available for this paper at https://doi.org/10.1038/s41565-018-0267-z.

Reprints and permissions information is available at www.nature.com/reprints.

Correspondence and requests for materials should be addressed to P.Y.

Publisher's note: Springer Nature remains neutral with regard to jurisdictional claims in published maps and institutional affiliations.

Methods

Preparation of AuNCs. The red-emitting AuNCs were synthesized by a pH-mediated $NaBH_4$ reduction method. In a typical synthesis, aqueous solutions of $HAuCl_4$ (12.5 ml, 20 mM) and GSH (7.5 ml, 50 mM) were added to a 500-ml flask containing 180 ml of ultrapure water. After 2 min of vigorous stirring, the pH of the reaction solution was brought to 12.0 with 1 M NaOH. Thereafter, 0.24 mg $NaBH_4$ in 0.1 ml water was added into the reaction solution, stirring at 500 r.p.m. at room temperature. After 0.5 h, the solution pH was adjusted to 2.5 with 0.33 M HCl. The reaction solution was then sealed airtight and slowly stirred at 200 r.p.m. for 8 h. An aqueous solution of strong red-emitting AuNCs was formed. To isolate AuNCs from the solution, isopropyl alcohol was added with 1:1 volume ratio. The dark red precipitate was collected through high-speed centrifugation at 14,000 r.p.m. and washed with 1:1 methanol:H_2O mixture. Polyacrylamide gel electrophoresis (PAGE, 30 wt% monomers) was then applied to separate and collect $Au_{22}(SG)_{18}$ from $Au_{15}(SG)_{13}$ and $Au_{18}(SG)_{14}$ (Supplementary Fig. 8).

Preparation of heterotrophic medium and autotrophic medium. Both media were prepared under anaerobic conditions with deionized (DI) water. The Hungate technique or an anaerobic chamber (Coy) was used in all operations to prevent exposure of the anaerobic bacteria to oxygen. The recipe for a general broth is as follows: to a bottle of 1 l degassed DI water was added 400 mg NaCl, 400 mg NH_4Cl, 330 mg $MgSO_4{\cdot}7H_2O$, 50 mg $CaCl_2$, 250 mg KCl and 2.5 g $NaHCO_3$. The mixture was heated and stirred to boiling point under a continuous flux of nitrogen atmosphere, and 10 ml Wolfe's vitamin mix (Supplementary Table 2) and 10 ml trace mineral mix (Supplementary Table 3) were added after cooling to room temperature. To make the heterotrophic medium, 25 ml 1 M glucose solution, 20 ml 5 wt% Cys·HCl solution, 800 mg β-glycerophosphate·2Na·xH_2O, 500 mg yeast extract and 500 mg tryptone were added into 1 l of the general broth and stirred until fully dissolved. To make the autotrophic medium, 640 mg K_2HPO_4 was added into 1 l of the general broth. Yeast extract and tryptone were obtained from BD Biosciences, and all other reagents were obtained through Sigma-Aldrich. Anaerobic media were then dispensed under a mixed atmosphere (80:20 mixture of N_2:CO_2) into 16 × 125 mm Balch-type anaerobic culture tubes (Chemglass) with butyl rubber stoppers and screw caps, and 18 × 150 mm Balch-type anaerobic culture tubes (Chemglass) with butyl rubber stoppers and aluminium crimp seals. Media were then autoclaved for 15 min at 121 °C before use.

Growth of *M. thermoacetica*/AuNCs. The initial inoculum of *M. thermoacetica* (ATCC 39073) was cultured in the heterotrophic medium, and the late log cultures were cryopreserved in a −80 °C freezer with 10% dimethyl sulfoxide as a cryoprotectant. To prepare *M. thermoacetica*/AuNC hybrids, the thawed cryopreserved stock of 10 ml *M. thermoacetica* was inoculated in 10 ml of the anaerobic heterotrophic medium at 5 vol%, and incubated with occasional agitation at 52 °C. The headspace of each tube was pressurized to 150 kPa with a flux of the mixed atmosphere (80:20 mixture of N_2:CO_2). After 2 days of growth (OD_{600} = 0.16), the culture was reinoculated at 5 vol% into fresh heterotrophic medium, and incubated at 52 °C. After 36 hours of growth (OD_{600} = 0.28), 0.5 ml of 4 mg ml^{-1} $Au_{22}(SG)_{18}$ solution was added to each tube. The chemical stability of AuNCs at different concentrations was tested by UV–vis absorption, and the intracellular AuNC stability was also explored through the SIM emission intensity (Supplementary Fig. 9). The tubes were returned to incubation and placed in the mini shaker (VMR) at a speed of 100 r.p.m. for 1 h, and then stood still for the rest days without shaking. After an additional 1 day, each tube was centrifuged at 2,500 r.p.m. for 10 min, washed and resuspended in an equivalent volume of autotrophic medium supplemented with 0.1 wt% cysteine. We distributed 10 ml of the suspension into each clean anaerobic tube equipped with a magnetic stir bar (sealed and autoclaved as previously described). Each tube was pressurized with 150 kPa of 80:20 H_2:CO_2 and incubated for 12 hours at 52 °C to promote autotrophic respiration.

Photosynthesis measurements. Prior to photosynthesis, the mixed flux of 80:20 N_2:CO_2 was continuously applied to each tube for 5 mins to extrude the residual mixture of H_2 and CO_2. An additional 0.1 wt% cysteine was then added to each tube (total 0.2 wt%, nominal). Each tube was stirred at 150 r.p.m. and heated to a measured temperature of 55 °C by a stirring hot plate. The illumination source used for simulated sunlight measurements was a collimated 75 W Xenon lamp (Newport) with an AM 1.5 G filter. All light intensities were calibrated by a silicon photodiode (Hamamatsu S1787-04). Concentrations of photosynthetic products were measured by ^{1}H-qNMR with sodium 3-(trimethylsilyl)-2,2′,3,3′-tetradeuteropropionate (TMSP-d_4, Cambridge Isotope Laboratories) as the internal standard in D_2O. Spectra were processed using the MestReNova software. The experiments for all the conditions were replicated, and the sample sizes are listed in Figs. 3 and 4. The ^{13}C isotope labelling experiments were conducted in the autotrophic medium with $NaH^{13}CO_3$, and the headspace was pressurized by $^{13}CO_2$. Photosynthetic products were measured by ^{1}H-NMR and ^{13}C-NMR.

Optical characterization. The UV–vis spectra of *M. thermoacetica*/AuNC suspensions were obtained with a UV–vis–NIR spectrophotometer (Shimadzu UV3101PC) with an integrating sphere. Photoluminescence spectra were taken in a confocal fluorescence spectroscope based on a Horiba LabRAM HR system. Excitation solid-state laser illumination at wavelength 532 nm was focused onto the sample by an optical objective (×20 magnification, numerical aperture 0.4). Fluorescence from the sample was collected by the same objective and sent to the spectroscope for analysis. The spectroscope was equipped with a diffraction grating of 600 lines mm^{-1} (blaze wavelength at 500 nm) and a charge-coupled device (CCD) camera.

SIM microscopy. Super-resolution 3D-SIM imaging was performed on an ELYRA PS.1 system (Zeiss). Images were acquired with a 100×/1.40 oil immersion objective (Plan-Apochromat) and an iXon 885 electron microscope CCD camera (Andor). A 100-mW, 540-nm optically pumped semiconductor laser (Coherent) and a BP 570/650-nm emission filter (Optics Balzers) were used. Twenty-eight images per plane (three rotations) and 86-nm *z* sections of total height 2.4 μm were acquired for generating super-resolution images. Raw images were reconstructed and processed to demonstrate structure with greater resolution by ZEN 2011 software (Zeiss). The Imaris software was used to analyse the reconstructed images.

Electron microscopy. Samples of fixed *M. thermoacetica*–CdS and *M. thermoacetica*/AuNCs were prepared for STEM by dropping the fixed suspension on Formvar-coated ultrathin-carbon/copper transmission electron microscope grids, settling for 1 hour and washing briefly in DI water. Grids were air-dried overnight. STEM imaging and EDS mapping was performed at 80 kV with an FEI Titan microscope at the National Center for Electron Microscopy (NCEM). The EDS signal was acquired with a windowless detector (FEI SuperX Quad) based on silicon drift technology that was controlled by Bruker Esprit software.

Viability test. Cell density (cells ml^{-1}) values were determined by manual counting with a Petroff–Hauser counting chamber in both dark and light conditions. In parallel, colony-forming unit (CFU) assays were performed by sampling and inoculating 0.1 ml of the *M. thermoacetica*, *M. thermoacetica*–CdS and *M. thermoacetica*/AuNC photosynthesis suspension into 5 ml of molten (temperature $T > 50$ °C) agar broth supplemented with 40 mM glucose and 0.1 wt% cysteine to double-check the viability. After thorough mixing, the anaerobic tubes were placed horizontally in ice to set a thin layer of agar on their sidewalls. Assay tubes were pressurized to 150 kPa with 80:20 N_2:CO_2 and incubated vertically at 52 °C. After 3 days of growth, visible white circular colonies were counted to determine the CFU per millilitre as a measure of cell number and viability in the light. In the meantime, the viability of *M. thermoacetica*/AuNCs with different AuNC concentrations in the dark was measured (Supplementary Table 4).

ROS assay test. Fluorometric Intracellular ROS Assay MAK143 Kit was cultured with *M. thermoacetica*/AuNCs for sensitive, one-step fluorometric to detect intracellular ROS (especially superoxide and hydroxyl radicals) in live cells within 1 hour incubation. The medium was as the control. The analysis was performed 12 and 48 after the illuminated in autotrophic medium. The 96 well with clear bottom black plate was used for fluorometric emission (λ_{ex} = 490/λ_{em} = 520 nm). The relative luminescence units were measured by a plate reader (DTX 880, Beckman Coulter).

Data availability

The data that support the plots within this paper and other findings of this study are available from the corresponding author upon reasonable request.

nature research

Corresponding author(s): NNANO-18030469A

Reporting Summary

Nature Research wishes to improve the reproducibility of the work that we publish. This form provides structure for consistency and transparency in reporting. For further information on Nature Research policies, see Authors & Referees and the Editorial Policy Checklist.

Statistical parameters

When statistical analyses are reported, confirm that the following items are present in the relevant location (e.g. figure legend, table legend, main text, or Methods section).

n/a	Confirmed	
☐	☒	The exact sample size (*n*) for each experimental group/condition, given as a discrete number and unit of measurement
☐	☒	An indication of whether measurements were taken from distinct samples or whether the same sample was measured repeatedly
☒	☐	The statistical test(s) used AND whether they are one- or two-sided *Only common tests should be described solely by name; describe more complex techniques in the Methods section.*
☐	☒	A description of all covariates tested
☒	☐	A description of any assumptions or corrections, such as tests of normality and adjustment for multiple comparisons
☐	☒	A full description of the statistics including central tendency (e.g. means) or other basic estimates (e.g. regression coefficient) AND variation (e.g. standard deviation) or associated estimates of uncertainty (e.g. confidence intervals)
☒	☐	For null hypothesis testing, the test statistic (e.g. *F*, *t*, *r*) with confidence intervals, effect sizes, degrees of freedom and *P* value noted *Give P values as exact values whenever suitable.*
☒	☐	For Bayesian analysis, information on the choice of priors and Markov chain Monte Carlo settings
☒	☐	For hierarchical and complex designs, identification of the appropriate level for tests and full reporting of outcomes
☒	☐	Estimates of effect sizes (e.g. Cohen's *d*, Pearson's *r*), indicating how they were calculated
☐	☒	Clearly defined error bars *State explicitly what error bars represent (e.g. SD, SE, CI)*

Our web collection on statistics for biologists may be useful.

Software and code

Policy information about availability of computer code

Data collection	Zeiss ELYRA PS.1.
Data analysis	ZEN 2011 and MestReNova software were used for data analysis

For manuscripts utilizing custom algorithms or software that are central to the research but not yet described in published literature, software must be made available to editors/reviewers upon request. We strongly encourage code deposition in a community repository (e.g. GitHub). See the Nature Research guidelines for submitting code & software for further information.

Data

Policy information about availability of data

All manuscripts must include a data availability statement. This statement should provide the following information, where applicable:

- Accession codes, unique identifiers, or web links for publicly available datasets
- A list of figures that have associated raw data
- A description of any restrictions on data availability

The data that support the plots within this paper and other findings of this study are available from the corresponding author upon reasonable request.

Field-specific reporting

Please select the best fit for your research. If you are not sure, read the appropriate sections before making your selection.

☒ Life sciences ☐ Behavioural & social sciences ☐ Ecological, evolutionary & environmental sciences

For a reference copy of the document with all sections, see nature.com/authors/policies/ReportingSummary-flat.pdf

Life sciences study design

All studies must disclose on these points even when the disclosure is negative.

Sample size	M. thermoacetica (ATCC 39073) was the only bacterial strain used in the experiments, and the sample size for each condition is around 20-35 culture batches.
Data exclusions	No data were excluded from the analysis
Replication	For all biological experiments, more than three repeats were performed and the results were reproducible. (The culture number was listed for each condition)
Randomization	Not relevant. There is only one type bacterial strain used in laboratory experiments.
Blinding	The study works with bacterial strain and there is no reason for blinding.

Reporting for specific materials, systems and methods

Materials & experimental systems

n/a	Involved in the study
☒	☐ Unique biological materials
☒	☐ Antibodies
☒	☐ Eukaryotic cell lines
☒	☐ Palaeontology
☒	☐ Animals and other organisms
☒	☐ Human research participants

Methods

n/a	Involved in the study
☒	☐ ChIP-seq
☒	☐ Flow cytometry
☒	☐ MRI-based neuroimaging